JOC The Journal of Organic Chemistry

Article

pubs.acs.org/joc

Theoretical Study of Gold-Catalyzed Cyclization of 2-Alkynyl-*N*-propargylanilines and Rationalization of Kinetic Experimental Phenomena

Yeqing Duan, Yuxia Liu, Siwei Bi,* Baoping Ling, Yuan-Ye Jiang, and Peng Liu

School of Chemistry and Chemical Engineering, Qufu Normal University, Qufu 273165, People's Republic of China

Supporting Information

ABSTRACT: Gold-catalyzed cyclization of 2-alkynyl-*N*-propargylanilines provides a step-economic method for the construction of three-dimensional indolines. In this article, the M06 functional of density functional theory was employed to gain deeper insights into the reaction mechanism and the associated intriguing experimental observations. The reaction was found to first undergo Au(I)-induced cyclization to form an indole intermediate, 1,3-propargyl migration, and substitution with the substrate 2-alkynyl-*N*-propargylaniline (**R1**) to generate the intermediate product **P1**, an allene species. Subsequently, Au(I)-catalyzed conversion of **P1** into the final product **P2**, an indoline compound, occurs first through direct cyclization rather than via the previously proposed four-membered carbocycle intermediate. Thereafter, water-assisted oxygen heterocycle formation and proton transfer generate the final product. The calculated activation free energies indicate that **P1** formation is 5.9 times slower than **P2** formation, in accordance with the fact that **P1** formation is rate-limiting. Futhermore, the intriguing experimental phenomenon that **P2** can be accessed only after almost all the substrate **R1** converts to **P1** although **P1** formation is rate-limiting was rationalized by employing an energetic span model. We found the initial facile cyclization to form a highly stable indole intermediate in the formation of **P1** is the key to the intriguing experimental phenomenon.

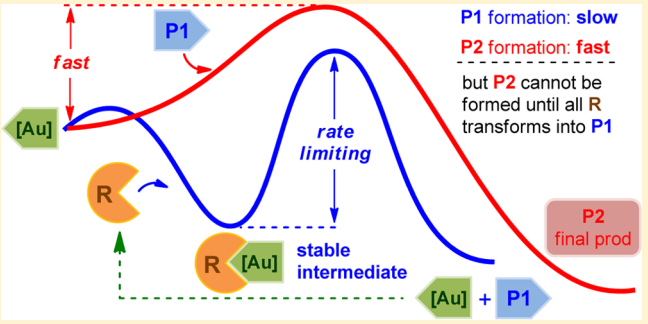

1. INTRODUCTION

Due to the strong relativistic effect of gold,[1] gold catalysts are found to be of soft and carbophilic character, high π-acidity, and high tolerance of functional groups.[2] Homogeneous gold catalysts have emerged as a powerful strategy for generating carbocycles and heterocycles, which are especially applicable to the synthesis of natural products and complex molecules.[3] These catalytic transformations with remarkably high efficiencies are initiated from the polarization of nonpolar unsaturated carbon−carbon bonds through gold π-coordination. A variety of efficient Au-catalyzed reactions, including hydroalkoxylation,[4] hydroamination,[4c,5] and hydroarylation,[4c,6] have been developed. Nevertheless, reports on the cyclization reactions with substrates bearing two nucleophilic sites[7] are still limited. Recently, the Fujii and Ohno group developed a class of reactions of 2-alkynyl-*N*-propargylaniline that accessed fused three-dimensional indolines in a single operation, involving four bonds and three rings formed (Scheme 1).[8] The Au(I)-catalyzed isomerizations of 2-alkynyl-*N*-propargylaniline into indolines were demonstrated to be highly functionally tolerant under mild reaction conditions. Particularly, 1,3-migration of the propargyl group is involved in these transformations, which is the first example of the propargyl migration from the aniline nitrogen atom and application to cascade cyclizations.

In these Au(I)-catalyzed isomeric transformations of 2-alkynyl-*N*-propargylaniline, an intermediate allene product was found to be first formed, and then the final indoline product was produced via a series of nucleophilic addition steps. The allene product formation was demonstrated experimentally to be rate-limiting, while the following process generating the final indoline product was fast. However, an intriguing experimental observation was found in which the conversion of the intermediate product **P1** to final product **P2** only takes place until almost all of the substrate **R1** catalytically converts to the intermediate product **P1** (Scheme 2). In other words, once the intermediate product is formed, it cannot convert to the final product immediately, although the final product formation is more facile than the allene product formation. This experimental phenomenon is in contrast to the general belief

Scheme 1. Au-Catalyzed Cyclization of 2-Alkynyl-*N*-propargylaniline

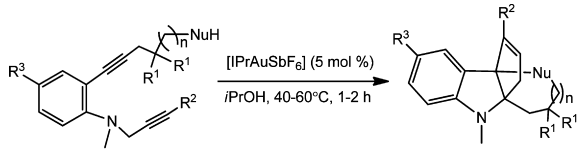

R^1 = H, Me, CH_2Cl; R^2 = H, Me, Et, Ph; R^3 = H, Me, OMe, Br, F; Nu = O, NTs, NBoc

Received: August 25, 2016
Published: September 7, 2016

DOI: 10.1021/acs.joc.6b02092
J. Org. Chem. 2016, 81, 9381−9388

Scheme 2. Kinetic Observations of Au-Catalyzed Cyclization of 2-Alkynyl-*N*-propargylaniline

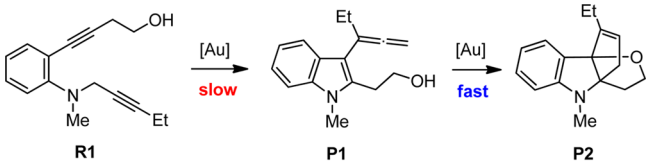

But **P2** cannot be formed until almost all **R1** transforms into **P1**

that, once the first product is formed through a rate-limiting process, it would quickly convert to the more stable final product.

Associated with the rapid development of experimental methodologies, mechanistic studies on Au-catalyzed cyclization are drawing extensive attention in recent years.[9] Herein, DFT studies were performed to address the mechanism of the first example of Au-catalyzed propargyl migration from the aniline nitrogen. Based on the calculation results, we expect to rationalize the "counter-generally-believed" experimental phenomenon, and furthermore, to establish an approach to predict under what conditions (1) final product formation takes place after intermediate product completely formed, (2) both intermediate and final products are formed simultaneously at the similar reaction rate, and (3) final product formation quickly takes place once intermediate product is formed.

2. COMPUTATIONAL DETAILS

The reaction in eq 1 was chosen as a typical prototype in this study. Molecular geometries of all complexes studied were optimized at the

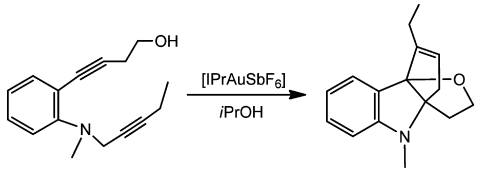

(1)

M06 level of density functional theory.[10] Frequency calculations at the same level of theory were also performed to identify all of the stationary points as minima (zero imaginary frequencies) or transition states (one imaginary frequency) and to provide free energies at 298.15 K. Intrinsic reaction coordinates[11] were carried out to identify transition states connecting two relevant minima. For geometry optimization and frequency analysis, the effective core potentials of Hay and Wadt with a double-ζ valence basis set (LanL2DZ)[12] were chosen to describe the Au atom. In addition, the polarization function was added for Au ($\zeta_f = 1.05$).[13] The 6-31g(d,p)[14] basis set was used for all other atoms, including C, H, N, and O.

To consider the solvent effect, we also employed a continuum medium to do single-point calculations for all species using UAKS radii on the polarizable continuum model.[15] Single-point energies were obtained in solution using the M06 functional with the SDD[16] pseudopotential for Au and with the 6-311G(d,p) basis set for all other atoms. Acetonitrile was employed as the solvent, corresponding to the reaction conditions. Although the B3LYP[17] functional has been employed to computationally study gold catalysis systems, the M06[18] functional was chosen to be used in this work based on the fact that this functional estimates the van der Waals interactions more precisely.[19] In all of the figures that contain potential energy profiles, solvation-corrected relative free energies and enthalpy energies (in parentheses) were presented. In this paper, the solvation-corrected relative free energies were used to analyze the reaction mechanisms. Unless otherwise stated, the Gibbs free energies obtained in solution are used in our discussion. All calculations were performed with the Gaussian 09 software package.[20] Partial atomic charges were calculated on the basis of natural bond orbital (NBO) analyses,[21] where the basis sets, SDD for Au and 6-311G(d,p) for other atoms, are employed.

3. RESULTS AND DISCUSSION

We first investigate the detailed reaction mechanism leading to the intermediate product **P1**, an allene compound, and then explore the mechanism from the intermediate product **P1** to the final product **P2**, an indoline compound. Finally, we expect to establish an approach from a theoretical point of view to rationalize the "counter-generally-believed" and other "generally-believed" experimental phenomena that would be possibly observed in this type of reactions.

3.1. Mechanistic Study of the Formation of Allene Product P1. Au(I) complexes prefer a linear two-coordinate structure, which has been demonstrated in previous reports.[22] In the $IPrAuSbF_6$ catalyst, the anionic SbF_6^- is found to have little impact on the reactions,[16b,23] and thus the cationic $IPrAu^+$ is employed as the active catalyst in studying the reaction in eq 1. On the basis of the possible reaction pathways proposed by Fujii and Ohno, the free energy profile calculated for generating the allenic product (**P1**) is shown in Figure 1. Selected

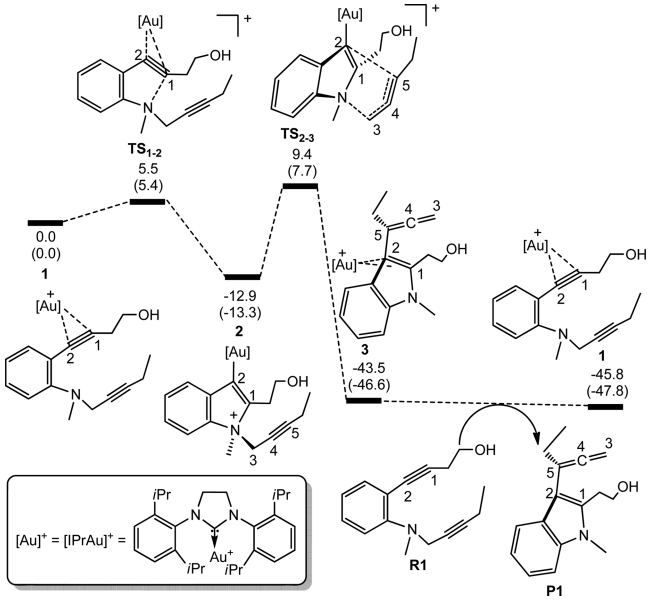

Figure 1. Gibbs free energy profile calculated for $[(IPr)Au]^+$-catalyzed formation of the allene product **P1**. The free energies and the enthalpies in parentheses are given in kcal/mol.

geometric structures together with key structural parameters are presented in Figure 2. Since the Au-coordinated species **1** is significantly lower in energy than the separate gold catalyst $[IPrAu]^+$ and 2-alkynyl-*N*-propargylaniline (**R1**), **1** is set to be the zero reference point. The first step (**1** → **2**) is the Au-induced nucleophilic cyclization to give indole **2**. As seen from the TS_{1-2} transition states' geometric structure, the nitrogen atom nucleophilically attacks the acetylenic atom C1, with the calculated N···C1 distance being 2.566 Å (Figure 2). The binding of gold with the carbon−carbon triple bond switches from η^2 to the η^1 mode. This step features the formation of the new N−C1 bond, and because of this bond formation, the N−C3 bond is found to be weakened appreciably. As shown in Figure 2, the N−C3 bond length is elongated to 1.528 Å in **2** from 1.471 Å in **1**. NBO computations show that the Wiberg bond index of this bond is decreased to 0.84 in **2** from 0.94 in

DOI: 10.1021/acs.joc.6b02092
J. Org. Chem. 2016, 81, 9381−9388

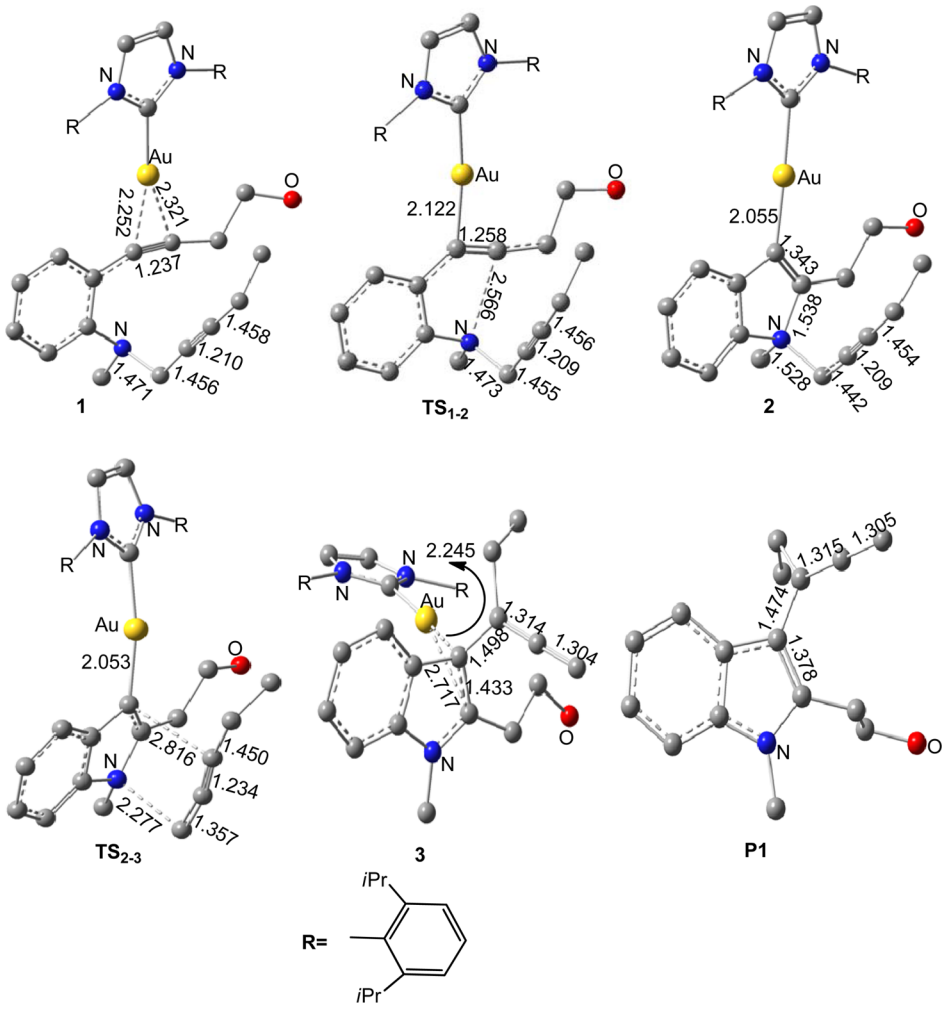

Figure 2. Optimized structures of selected species shown in Figure 1, together with key structural parameters. For clarity, the hydrogen atoms are omitted. The bond distances are given in Å.

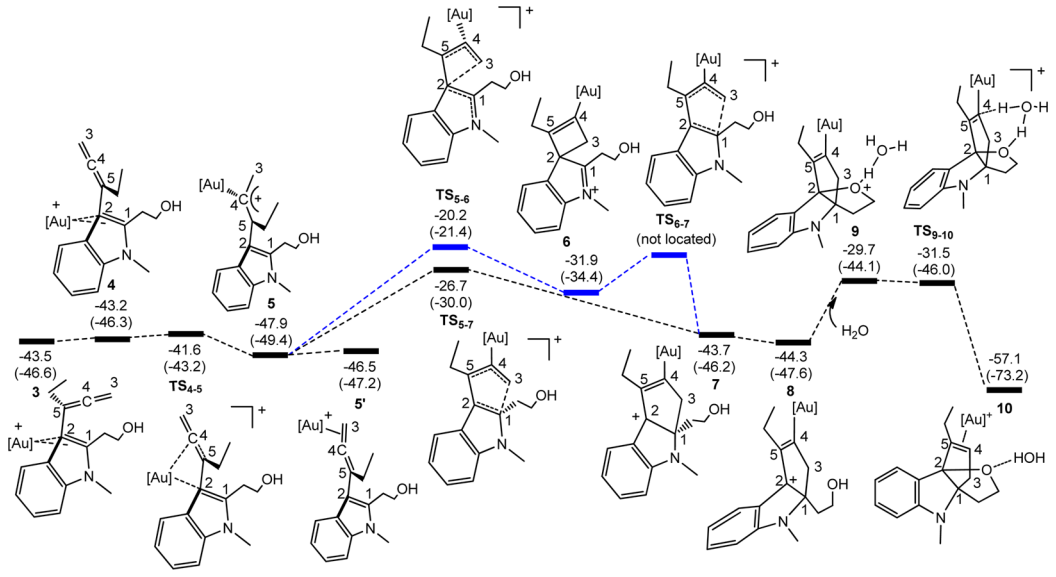

Figure 3. Gibbs free energy profile calculated for [(IPr)Au]$^+$-catalyzed formation of the indoline product **P2**. The free energies and the enthalpies in parentheses are given in kcal/mol.

1. Importantly, the activation of the N−C3 bond favors the 1,3-propargyl migration that will occur in the next step. This step is kinetically accessible with the calculated activation barrier being only 5.5 kcal/mol. The resulting indole **2** is more stable than **1**

DOI: 10.1021/acs.joc.6b02092
J. Org. Chem. 2016, 81, 9381−9388

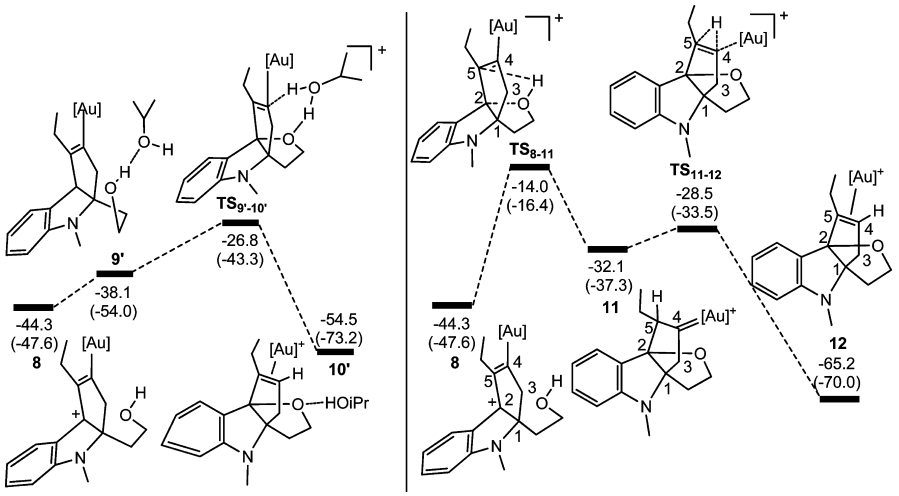

Figure 4. Gibbs free energy profiles associated with the formation of the indoline product **P2** from intermediate **8**. Left: *i*PrOH serving as a shuttle. Right: direct 1,2-migration of the proton. The free energies and the enthalpies in parentheses are given in kcal/mol.

by 12.9 kcal/mol due to formation of the five-membered heterocycle, which is found to be crucial in preventing **P2** formation before all of the substrate converts to the allene product **P1** (although **P2** formation is faster than **P1** formation).

As mentioned by Fujii, Ohno, and co-workers, their experimental work represents the first example of the migration of a propargyl substituent from the aniline nitrogen atom. Step **2** → **3** shown in Figure 1 is related to 1,3-migration of a propargyl substituent, giving the allenic gold complex **3**. The activation barrier for the propargyl migration is calculated to be 22.3 kcal/mol, well within the range expected for a reaction that proceeds under mild conditions (40 °C). The relatively low activation barrier can be mainly ascribed to the two factors. One is the N−C3 bond activation in **2** as a result of the N−C1 bond formation as mentioned above. Electron density decrease at the nitrogen atom weakens the N−C3 bond. The other is the resulting relative stability of the propargyl moiety in $\mathbf{TS}_{2-3}$. The C3 atom in **2** adopts sp^3 hybridization, while in $\mathbf{TS}_{2-3}$, it switches to sp^2. In other words, a conjugation is being formed among C3, C4, and C5 atoms, as supported by structural parameters and the NBO charges. The C3−C4 bond is shortened to a nearly double bond distance of 1.357 Å in $\mathbf{TS}_{2-3}$ from 1.442 Å in **2**. The NBO charge at C5 is increased to 0.220 in $\mathbf{TS}_{2-3}$ from 0.115 in **2**, suggesting that the π-electrons slip from C4−C5 to C3−C4. In summary, the appreciable N−C3 bond activation caused by N−C1 bond formation and the resulting stability of the migrating propargyl moiety caused by effective conjugation enable $\mathbf{TS}_{2-3}$ to not be very high in energy, although the propargyl is still far away from the Au-bonded C2 atom (C2−C5, 2.816 Å) in the transition state. In the last step, a ligand exchange process takes place, with the allene product **P1** being obtained and the starting intermediate **1** being regenerated. Our calculation results confirmed that the Au(I)-catalyzed formation of the allene product **P1** is both kinetically and thermodynamically accessible, supporting the experimental observations.

3.2. Mechanistic Study of the Formation of Indoline Product P2. As described above, allene product **P1** can be obtained through nucleophilic cyclization, 1,3-propargyl migration, and ligand exchange. The experiments also demonstrated the formation of the final indoline product **P2** when the reaction time is prolonged. Detailed free energy profiles calculated for the process from **3** to **P2** are shown in Figure 3, and the optimized structures of selected species together with key structural parameters are presented in Figure S1 in the Supporting Information. Step **3** → **4** involves a simple conformation change about the C2−C5 bond rotation, which enables the allene moiety proximal to the gold catalyst. This step is necessary for subsequent electrophilic attack of the cationic gold toward the allene moiety. Step **4** → **5** is found to be a transformation from η^2-C1═C2 coordination with Au(I) to form an allylic cation (the Au−C4 bond length is 2.119 Å), with an activation barrier of only 1.6 kcal/mol. The NBO charges calculated at C1, C2, C5, C4, and C3 are 0.377, −0.198, 0.176, −0.347, and −0.374, respectively, suggesting that C1 and C5 are more positively charged. The authors[8] suggested a slippage from (η^2-C1═C2) → Au in **4** to (η^2-C3═C4) → Au to afford intermediate **5′**, which is slightly less stable than **5**. The gold(I) catalyst renders the linear allene moiety in **4** into a bent structure in **5**, favoring the subsequent cyclization process. **5′** is not favored for subsequent cyclization because the C3−C4−C5 in **5′** becomes closer to linearity and the (η^2-C3═C4) → Au coordination makes C3 less nucleophilic. The next step (**5** → **7**) is related to a cyclization process via C3−C1 bond formation, generating a five-membered carbocyclic intermediate **7**. Experimentally, the authors proposed generation of intermediate **7** by undergoing a four-membered carbocyclic intermediate **6** followed by ring expansion. The transition state $\mathbf{TS}_{5-6}$ for formation of the four-membered carbocyclic intermediate **6** was located with an activation barrier of 27.7 kcal/mol, which is obviously higher than the one related to the propargyl migration (**2** → $\mathbf{TS}_{2-3}$, 22.3 kcal/mol). Clearly, the computational results indicate that the pathway via **6** to **7** contradicts the experimental fact that formation of **P1** in the first catalytic state is rate-limiting. Thus, a more reasonable pathway leading to **7** is expected. A direct formation of the five-membered carbocyclic intermediate **7** from **5** is proposed. As shown in transition state $\mathbf{TS}_{5-7}$, the terminal allenic C3 is directly nucleophilically attacking at the N-bonded C1 atom, aiming to form a C3−C1 bond. $\mathbf{TS}_{5-7}$ is significantly more stable than $\mathbf{TS}_{5-6}$ by 6.5 kcal/mol. Two factors contribute to the stability of $\mathbf{TS}_{5-7}$. One is that the ring strain involved in the four-membered ring (C2−C3−C4−C5) of $\mathbf{TS}_{5-6}$ is stronger

DOI: 10.1021/acs.joc.6b02092
J. Org. Chem. 2016, 81, 9381−9388

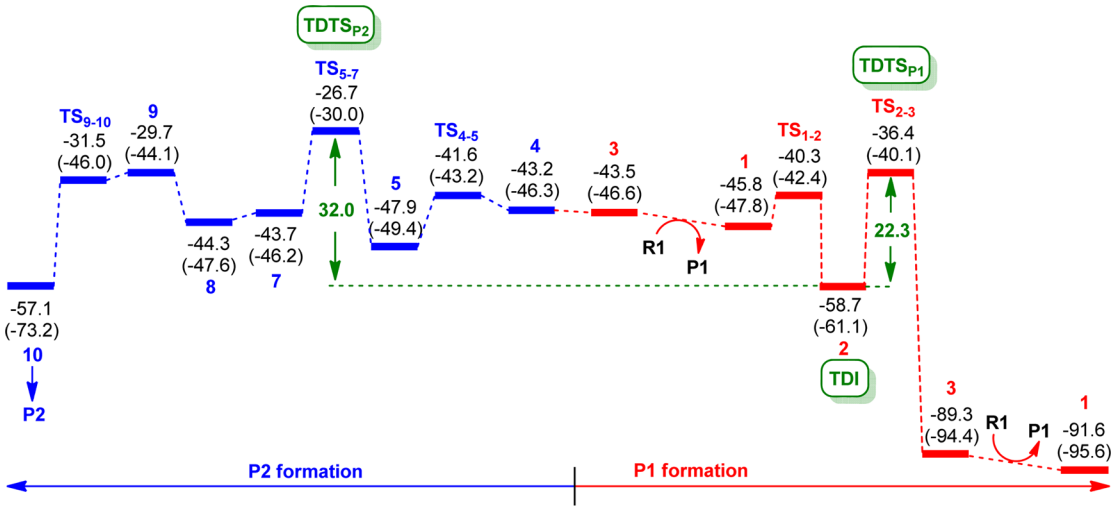

Figure 5. Gibbs free energy profile calculated for the whole [(IPr)Au]$^+$-catalyzed reaction leading to formation **P1** and **P2** (red and blue lines, respectively). The free energies and the enthalpies in parentheses are given in kcal/mol.

than the one involved in the five-membered ring (C2−C1−C3−C4−C5) of $\mathbf{TS_{5-7}}$. The bond angle of C5−C4−C3 (101.7°) in $\mathbf{TS_{5-6}}$ is obviously smaller than the one in $\mathbf{TS_{5-7}}$ (C5−C4−C3: 112.1°). The other important factor is associated with the electronic interactions. As given above, the NBO charge of C3 in **5** is −0.374, indicating a nucleophilic character, whereas at the C1 and C2 atoms, the NBO charges are 0.377 and −0.198, respectively, indicating C1 is electrophilic and C2 is nucleophilic. C1 being positively charged is a result of its binding with the nitrogen atom. Therefore, nucleophilic attack of C3 toward C1 is clearly favored over the attack toward C2. Additionally, it is worth noting that the direct cyclization via $\mathbf{TS_{5-7}}$ proposed by us is consistent with the experimental fact that formation of **P1** is rate-liming in the whole reaction. The barrier from **5** to $\mathbf{TS_{5-7}}$ is 21.2 kcal/mol, lower than the barrier to the rate-limiting propargyl migration (22.3 kcal/mol).

The steps following intermediate **7** are associated with the generation of the oxygen heterocycle. Conformational change (**7** → **8**) through facile σ-bond rotation makes the hydroxyl oxygen proximal to C2, favoring subsequent C2−O bond formation. From **8**, three pathways leading to **P2** can be proposed. The pathway with water serving as a shuttle is shown in Figure 3.[24] The pathways with no shuttle involved and with *i*PrOH acting as a shuttle are shown in Figure 4. Binding of **8** with water via a hydrogen bond affords intermediate **9**. The hydrogen bond weakens the hydroxyl O−H bond and consequently strengthens the O−C2 interaction. As the calculated results show from **8** to **9**, the O−C2 bond is dramatically shortened from 2.999 to 1.609 Å and the hydroxyl O−H bond is elongated from 0.963 to 1.011 Å. As a consequence, the subsequent proton transfer becomes significantly facile with water acting as a shuttle. The activation barrier calculated for this elementary step is as low as −1.8 kcal/mol, while the corresponding overall free energy barrier is 14.6 kcal/mol (refers to **8**).[25] The calculated overall free energy barrier is close to that in the recent study by Yates and co-workers on $(H_2O)_2H_3O^+$-induced protodeauration of Au(I) complexes.[26] After the transition state $\mathbf{TS_{9-10}}$, the migrating proton replaces the Au(I) catalyst to form a C4−H bond, and the Au(I) catalyst binds with the carbon−carbon double bond in an η^2-fashion, generating intermediate **10**. The relative free energy of $\mathbf{TS_{9-10}}$ is calculated to be −31.5 kcal/mol. Release of the catalyst and water gives the indoline product **P2**. For the pathway with *i*PrOH acting as a shuttle (Figure 4), the calculated free energy of the hydrogen transfer transition state $\mathbf{TS_{9'-10'}}$ is −26.8 kcal/mol, higher than that of $\mathbf{TS_{9-10}}$. For the pathway with direct hydrogen migration (Figure 4), the transition state of hydrogen transfer $\mathbf{TS_{8-11}}$ is found to be even higher in free energy (−14.0 kcal/mol). It should be noted that in the direct proton transfer process, the proton is found through our calculations to prefer attacking the β-carbon (C5) rather than attacking the α-carbon (C4). Then the proton migrates to C4 from C5 to afford the Au-coordinated allene product. Our calculated results predicted that involvement of a shuttle (e.g., water or *i*PrOH) can promote the hydrogen transfer from oxygen to the Au-bonded carbon atom. Compared with the two shuttles (water and *i*PrOH), water is predicted to be more efficient at promoting the hydrogen transfer.

In summary, our findings from investigating the reaction mechanism are as follows. (1) The propargyl migration to afford the Au(I)-coordinated allene product **3** is facilitated by formation of the nitrogen heterocycle. (2) Au(I) electrophilic attack toward the middle carbon atom of the allene moiety affords the Au−C4 σ-bond that makes hybridization of C4 switch from sp to sp^2, in favor of the upcoming carbocycle formation. (3) The five-membered carbocycle is generated via a direct cyclization rather than via a four-membered carbocyclic unit. (4) The proton transfer involved in forming the oxygen heterocycle is promoted by protic solvents. (5) The propargyl migration step is calculated to be rate-limiting, consistent with the experimental facts that formation of **P1** is slow and the transformation of **P1**→ **P2** is fast.

3.3. Explanation for the Unusual Experimental Observations. Fujii et al. observed that the yield of intermediate product **P1** continues to increase at the first time period at 40 °C. After 165 min, the yield of **P1** reaches 95%, while only 4% of the substrate remains. When the reaction time is further lengthened, **P2** begins to form and its yield reaches 93% after 50 min. Therefore, the **P1** formation can be roughly estimated to be 3.3 times slower than **P2** formation. In other words, the formation of **P1** is rate-limiting rather than that of **P2** in the whole catalytic process. The calculation activation free energy barrier for **P1** formation in Figure 1 is

DOI: 10.1021/acs.joc.6b02092
J. Org. Chem. 2016, 81, 9381−9388

22.3 kcal/mol (from **2** to $\mathbf{TS_{2-3}}$), and that for **P2** formation in Figure 3 is 21.2 kcal/mol (from **5** to $\mathbf{TS_{5-7}}$). These results predict that **P1** formation is slower than **P2** formation by 5.9 times at 40 °C if they occur individually, which are in accord with the above experimental observations. A general belief for the stoichiometric cascade reaction is that, once an intermediate product is generated through a rate-limiting process, it would quickly undergo subsequent steps to complete the whole reaction, giving the final product. Related experimental[27] and computational[28] studies have also supported this concept, in which the intermediate product formed through a rate-limiting step and the final product formed through subsequent steps were found present synchronously. Nevertheless, it is noted that Fujii et al. observed that the generation of **P2** was only allowed after almost all of the substrate catalytically converts to intermediate product **P1**, which is contrary to the general belief mentioned above. Therefore, there is something different between catalytic reactions and stoichiometric reactions. To give a rational explanation from a theoretical point of view for such a puzzling experimental phenomenon, we summarize the whole free energy profiles leading to **P1** and **P2** in Figure 5 (the red and blue lines, respectively). As seen from Figure 5, after intermediate **3** is afforded in the first catalytic cycle of **P1** formation, two pathways are competitive in the following transformations. One is the continuous generation of **P1** through the second cycle (the red line), and the other leads to **P2** (the blue line). In view of the results that $\mathbf{TS_{5-7}}$ is clearly higher in energy than $\mathbf{TS_{2-3}}$ by about 10 kcal/mol, the reaction prefers to undergo the path accessing **P1** rather than the one to **P2**. The reason for this result is that reaction of **3** with the substrate in the second cycle rapidly passes through $\mathbf{TS_{1-2}}$ to generate the stable intermediate **2**. The relatively high stability of **2** can, in part, be demonstrated by the experimental fact that a structurally similar *N*,*N*-dimethylindolylgold intermediate has been isolated.[29] In this case, once **P1** is formed, the gold catalyst is always trapped by the substrate to repeat generating **P1** until almost all of the substrate is consumed. From another point of view based on an energetic span model,[30] **2** is the common TOF-determining intermediate for both **P1** formation and **P2** formation; $\mathbf{TS_{2-3}}$ is the TOF-determining transition state for **P1** formation ($\mathbf{TSTS_{P1}}$), while $\mathbf{TS_{5-7}}$ is the TOF-determining transition state for **P2** formation ($\mathbf{TDTS_{P2}}$). The overall Gibbs free energy barrier for **P1** formation is 22.3 kcal/mol, whereas **P2** formation has an overall Gibbs free energy barrier of 32.0 kcal/mol. Therefore, **P2** could not be generated unless **P1** was completely consumed to avoid formation of **2**. Based on the above theoretical concept, the origin of Fujii et al.'s unusual experimental observations is clarified.

By employing the energetic span model, we can further roughly predict whether the accumulation of **P1** will be observed or not in other cases.[31] The TOF for **P1** formation and **P2** formation can be expressed as eqs 2 and 3, respectively.

$$\mathrm{TOF_{P1}} = \frac{K_B T}{h} e^{-\delta E_{P1}/RT} \tag{2}$$

$$\mathrm{TOF_{P2}} = \frac{K_B T}{h} e^{-\delta E_{P2}/RT} \frac{[P1]}{[R1]} \tag{3}$$

where K_B is the Boltzmann constant, T is the temperature, h is the Planck constant, R is the gas constant, [R1] is the concentration of the reactants, and [P1] is the concentration of **P1**. The term δE_{P1} is the relative Gibbs free energies difference between **2** and $\mathbf{TS_{2-3}}$, and δE_{P2} is the relative Gibbs free energies difference between **2** and $\mathbf{TS_{5-7}}$. Then, we can get the ratio of $\mathrm{TOF_{P1}}$ and $\mathrm{TOF_{P2}}$ as eq 4:

$$\frac{\mathrm{TOF_{P1}}}{\mathrm{TOF_{P2}}} = e^{\Delta G\mathbf{TS}_{5-7} - \Delta G\mathbf{TS}_{2-3}/RT} \frac{[R1]}{[P1]} \tag{4}$$

As shown in eq 4, the ratio of $\mathrm{TOF_{P1}}$ and $\mathrm{TOF_{P2}}$ is influenced by the relative Gibbs free energy difference between the two TDTSs, that is, $\mathbf{TS_{2-3}}$ and $\mathbf{TS_{5-7}}$. For our calculated energy profile, $\Delta G\mathbf{TS_{5-7}} - \Delta G\mathbf{TS_{2-3}}$ = 9.7 kcal/mol. Therefore, $\mathrm{TOF_{P1}}$ remains larger than $\mathrm{TOF_{P2}}$ when the reaction starts until [P1] is 5.9×10^6 times larger than [R1]. When [P1] is 100 times larger than [R1], $\mathrm{TOF_{P1}}$ is still 5.9×10^4 times larger than $\mathrm{TOF_{P2}}$ and 99% of **R1** has transformed into **P1** if the transformation of **P1** to **P2** is omitted during this time (because $\mathrm{TOF_{P1}}$ is much larger than $\mathrm{TOF_{P2}}$). In this situation, the accumulation of **P1** is expected to be observed. On the contrary, if $\Delta G\mathbf{TS_{5-7}}$ is significantly smaller than $\Delta G\mathbf{TS_{2-3}}$, for an example, $\Delta G\mathbf{TS_{5-7}} - \Delta G\mathbf{TS_{2-3}} = -5.0$ kcal/mol, $\mathrm{TOF_{P2}}$ becomes equal to $\mathrm{TOF_{P1}}$ when [R1] is 3.1×10^3 times larger than [P1]. When [P1] increases to 1/100 of [R1], $\mathrm{TOF_{P2}}$ becomes 31 times larger than $\mathrm{TOF_{P1}}$ and the generated **P1** will be quickly consumed to generate **P2**. On this occasion, the notable accumulation of **P1** will not be observed.

4. CONCLUSIONS

The reaction mechanism of gold-catalyzed cyclization of 2-alkynyl-*N*-propargylanilines was performed with the aid of density functional theory calculations. Two catalytic cycles in the whole reaction were clarified. The first cycle is related to Au-catalyzed formation of the intermediate allene product **P1** through the following steps: (a) Au-induced cyclization affording a N-containing five-membered ring intermediate **2**, (b) 1,3-propargyl migration generating an allene-coordinated gold complex **3**, and (c) substitution of the coordinated allene product in **3** with substrate **R1**, producing the allene product **P1**. The second cycle is associated with Au-catalyzed formation of the final product **P2**, a tetracyclic indoline, through the following steps: (a) bonding of Au(I) with the central allene carbon atom, making the carbon change from sp to sp^2, facilitating subsequent cyclization, (b) direct five-membered carbocycle formation rather than through a prior four-membered carbocycle formation, and (c) five-membered ring generation via O−C bond formation followed by protic-acid-assisted proton transfer producing **P2**. The calculated activation free energy indicates that formation of **P1** is 5.9 times slower than that of **P2** at 40 °C, which is well in accordance with the experimental observation that **P1** formation is rate-limiting in the whole catalytic reaction.

An intriguing phenomenon was observed experimentally. That is, the final product **P2** was accessed only after the almost all starting material was consumed, although formation of **P1** was rate-limiting. Our theoretical investigation reveals that the rapid reaction of the gold catalyst with the starting material to generate the highly stable intermediate **2** is the key for observation of intriguing phenomenon. Extensive predictions based on energetic span model were also provided in this study to describe how the relative stability of the TDTSs results in different experimental observations.

DOI: 10.1021/acs.joc.6b02092
J. Org. Chem. 2016, 81, 9381−9388

■ ASSOCIATED CONTENT

Supporting Information

The Supporting Information is available free of charge on the ACS Publications website at DOI: 10.1021/acs.joc.6b02092.

Complete ref 20, 3D structures of selected intermediates and transition states, Cartesian coordinates, and Gibbs free energies and enthalpies in solution for all of the calculated structures (PDF)

■ AUTHOR INFORMATION

Corresponding Author

*E-mail: siweibi@126.com.

Notes

The authors declare no competing financial interest.

■ ACKNOWLEDGMENTS

This work was supported by the National Natural Science Foundation of China (Nos. 21473100 and 21403123), Project of Shandong Province Higher Educational Science and Technology Program (No. J14LC17), Opening Foundation of Shandong Provincial Key Laboratory of Detection Technology for Tumor Makers (KLDTTM2015-9), and the Doctoral Start-Up Scientific Research Foundation of Qufu Normal University (Grant No. BSQD2012018).

■ REFERENCES

(1) Gorin, D. J.; Toste, F. D. *Nature* **2007**, *446*, 395−403.

(2) (a) Hashmi, A. S. K. *Chem. Rev.* **2007**, *107*, 3180−3211. (b) Li, Z.; Brouwer, C.; He, C. *Chem. Rev.* **2008**, *108*, 3239−3265. (c) Arcadi, A. *Chem. Rev.* **2008**, *108*, 3266−3325. (d) Jiménez-Núñez, E.; Echavarren, A. M. *Chem. Rev.* **2008**, *108*, 3326−3350. (e) Gorin, D. J.; Sherry, B. D.; Toste, F. D. *Chem. Rev.* **2008**, *108*, 3351−3378. (f) Patil, N. T.; Yamamoto, Y. *Chem. Rev.* **2008**, *108*, 3395−3442. (g) Kirsch, S. F. *Synthesis* **2008**, *2008*, 3183−3204.

(3) (a) Hashmi, A. S. K.; Rudolph, M. *Chem. Soc. Rev.* **2008**, *37*, 1766−1775. (b) Rudolph, M.; Hashmi, A. S. K. *Chem. Soc. Rev.* **2012**, *41*, 2448−2462.

(4) (a) Hashmi, A. S. K.; Schwarz, L.; Choi, J.-H.; Frost, T. M. *Angew. Chem., Int. Ed.* **2000**, *39*, 2285−2288. (b) Hoffmann-Röder, A.; Krause, N. *Org. Lett.* **2001**, *3*, 2537−2538. (c) Zhang, Z.; Liu, C.; Kinder, R. E.; Han, X.; Qian, H.; Widenhoefer, R. A. *J. Am. Chem. Soc.* **2006**, *128*, 9066−9073. (d) Gockel, B.; Krause, N. *Org. Lett.* **2006**, *8*, 4485−4488. (e) Zhang, Z.; Widenhoefer, R. A. *Angew. Chem.* **2007**, *119*, 287−289. (f) Alcaide, B.; Almendros, P.; Martinez del Campo, T. *Angew. Chem.* **2007**, *119*, 6804−6807. (g) Brown, T. J.; Weber, D.; Gagné, M. R.; Widenhoefer, R. A. *J. Am. Chem. Soc.* **2012**, *134*, 9134−9137. (h) Cox, N.; Uehling, M. R.; Haelsig, K. T.; Lalic, G. *Angew. Chem.* **2013**, *125*, 4978−4982.

(5) (a) Morita, N.; Krause, N. *Org. Lett.* **2004**, *6*, 4121−4123. (b) Lalonde, R. L.; Sherry, B. D.; Kang, E. J.; Toste, F. D. *J. Am. Chem. Soc.* **2007**, *129*, 2452−2453. (c) Zhang, Z.; Bender, C. F.; Widenhoefer, R. A. *J. Am. Chem. Soc.* **2007**, *129*, 14148−14149. (d) Kinder, R. E.; Zhang, Z.; Widenhoefer, R. A. *Org. Lett.* **2008**, *10*, 3157−3159. (e) Butler, K. L.; Tragni, M.; Widenhoefer, R. A. *Angew. Chem., Int. Ed.* **2012**, *51*, 5175−5178.

(6) (a) Liu, Z.; Wasmuth, A. S.; Nelson, S. G. *J. Am. Chem. Soc.* **2006**, *128*, 10352−10353. (b) Liu, C.; Widenhoefer, R. A. *Org. Lett.* **2007**, *9*, 1935−1938. (c) Watanabe, T.; Oishi, S.; Fujii, N.; Ohno, H. *Org. Lett.* **2007**, *9*, 4821−4824. (d) Weber, D.; Tarselli, M. A.; Gagné, M. R. *Angew. Chem., Int. Ed.* **2009**, *48*, 5733−5736. (e) Zeldin, R. M.; Toste, F. D. *Chem. Sci.* **2011**, *2*, 1706−1709. (f) Chen, B.; Fan, W.; Chai, G.; Ma, S. *Org. Lett.* **2012**, *14*, 3616−3619. (g) Ma, Z.-X.; He, S.; Song, W.; Hsung, R. P. *Org. Lett.* **2012**, *14*, 5736−5739.

(7) (a) Winter, C.; Krause, N. *Angew. Chem., Int. Ed.* **2009**, *48*, 6339−6342. (b) Alcaide, B.; Almendros, P.; Cembellín, S.; Martinez del Campo, T.; Fernández, I. *Chem. Commun.* **2013**, *49*, 1282−1284.

(8) Tokimizu, Y.; Oishi, S.; Fujii, N.; Ohno, H. *Angew. Chem., Int. Ed.* **2015**, *54*, 7862−7866.

(9) (a) Larsen, M. H.; Houk, K. N.; Hashmi, A. S. K. *J. Am. Chem. Soc.* **2015**, *137*, 10668−10676. (b) Yuan, R.; Lin, Z. *ACS Catal.* **2015**, *5*, 2866−2872. (c) Alcaide, B.; Almendros, P.; Fernández, I.; Martín-Montero, R.; Martínez-Peña, F.; Ruiz, M. P.; Torres, M. R. *ACS Catal.* **2015**, *5*, 4842−4845. (d) Zhang, Q.; Zhang, Z.-Q.; Fu, Y.; Yu, H.-Z. *ACS Catal.* **2016**, *6*, 798−808. (e) Alcaide, B.; Almendros, P. *Acc. Chem. Res.* **2014**, *47*, 939−952.

(10) (a) Neufeldt, S. R.; Jiménez-Osés, G.; Huckins, J. R.; Thiel, O. R.; Houk, K. N. *J. Am. Chem. Soc.* **2015**, *137*, 9843−9854. (b) Zhao, Y.; Truhlar, D. G. *Theor. Chem. Acc.* **2008**, *120*, 215−241. (c) Zhao, Y.; Truhlar, D. G. *Acc. Chem. Res.* **2008**, *41*, 157−167.

(11) (a) Fukui, K. *J. Phys. Chem.* **1970**, *74*, 4161−4163. (b) Fukui, K. *Acc. Chem. Res.* **1981**, *14*, 363−368.

(12) (a) Wadt, W. R.; Hay, P. J. *J. Chem. Phys.* **1985**, *82*, 284−298. (b) Hay, P. J.; Wadt, W. R. *J. Chem. Phys.* **1985**, *82*, 299−310.

(13) Ehlers, A. W.; Böhme, M.; Dapprich, S.; Gobbi, A.; Höllwarth, A.; Jonas, V.; Köhler, K. F.; Stegmann, R.; Frenking, G. *Chem. Phys. Lett.* **1993**, *208*, 111−114.

(14) Andzelm, J.; Huzinaga, S. *Gaussian Basis Sets for Molecular Calculations*; Elsevier Science: New York, 1984.

(15) (a) Barone, V.; Cossi, M. *J. Phys. Chem. A* **1998**, *102*, 1995−2001. (b) Cossi, M.; Rega, N.; Scalmani, G.; Barone, V. *J. Comput. Chem.* **2003**, *24*, 669−681. (c) Tomasi, J.; Mennucci, B.; Cammi, R. *Chem. Rev.* **2005**, *105*, 2999−3094.

(16) (a) Dolg, M.; Wedig, U.; Stoll, H.; Preuss, H. *J. Chem. Phys.* **1987**, *86*, 866−872. (b) Andrae, D.; Haußermann, U.; Dolg, M.; Stoll, H.; Preuß, H. *Theor. Chim. Acta.* **1990**, *77*, 123−141.

(17) (a) Shi, F.-Q.; Li, X.; Xia, Y.; Zhang, L.; Yu, Z.-X. *J. Am. Chem. Soc.* **2007**, *129*, 15503−15512. (b) Mauleón, P.; Krinsky, J. L.; Toste, F. D. *J. Am. Chem. Soc.* **2009**, *131*, 4513−4520. (c) Liu, Y.; Zhang, D.; Bi, S. *J. Phys. Chem. A* **2010**, *114*, 12893−12899. (d) Liu, Y.; Zhang, D.; Bi, S.; Liu, C. *Org. Biomol. Chem.* **2013**, *11*, 336−343. (e) Liu, Y.; Yang, X.; Liu, L.; Wang, H.; Bi, S. *Dalton. Trans.* **2015**, *44*, 5354−5363.

(18) (a) Felix, R. J.; Gutierrez, O.; Tantillo, D. J.; Gagné, M. R. *J. Org. Chem.* **2013**, *78*, 5685−5690. (b) Liang, H.; Bi, S.; Liu, Y.; Tang, Y. -n.; Liu, C. *Org. Biomol. Chem.* **2016**, *14*, 2637−2644.

(19) Sieffert, N.; Bühl, M. *Inorg. Chem.* **2009**, *48*, 4622−4624.

(20) Frisch, M. J.; et al. *Gaussian 09*, revision D.01; Gaussian, Inc.: Wallingford, CT, 2009. The full citation and computational details are given in the Supporting Information.

(21) (a) Glendening, E. D.; Reed, A. E.; Carpenter, J. E.; Weinhold, F. *NBO*, version 3.1. (b) Foster, J. P.; Weinhold, F. *J. Am. Chem. Soc.* **1980**, *102*, 7211−7218. (c) Reed, A. E.; Curtiss, L. A.; Weinhold, F. *Chem. Rev.* **1988**, *88*, 899−926.

(22) Gimeno, M. C.; Laguna, A. *Chem. Rev.* **1997**, *97*, 511−522.

(23) Alcaide, B.; Almendros, P.; Fernández, I.; Martín-Montero, R.; Martínez-Peña, F.; Ruiz, M. P.; Torres, M. R. *ACS Catal.* **2015**, *5*, 4842−4845.

(24) (a) Qu, S.; Dang, Y.; Song, C.; Guo, J.; Wang, Z.-X. *ACS Catal.* **2015**, *5*, 6386−6396. (b) Qu, S.; Dang, Y.; Song, C.; Wen, M.; Huang, K.-W.; Wang, Z.-X. *J. Am. Chem. Soc.* **2014**, *136*, 4974−4991. (c) Jiang, Y.-Y.; Yan, L.; Yu, H.-Z.; Zhang, Q.; Fu, Y. *ACS Catal.* **2016**, *6*, 4399−4410. (d) Yang, X. *ACS Catal.* **2014**, *4*, 1129−1133.

(25) For examples in which the Gibbs free energies of the connected intermediates are higher than transition states, see: (a) Dang, Y.; Qu, S.; Tao, Y.; Deng, X.; Wang, Z. − X. *J. Am. Chem. Soc.* **2015**, *137*, 6279−6291. (b) Dang, Y.; Qu, S.; Wang, Z. − X.; Wang, X. *J. Am. Chem. Soc.* **2014**, *136*, 986−998. (c) Li, Y.; Liu, S.; Qi, Z.; Qi, X.; Li, X.; Lan, Yu. *Chem. - Eur. J.* **2015**, *21*, 10131−10137. (d) Chen, W. − J.; Lin, Z. *Dalton Trans.* **2014**, *43*, 11138−11144.

(26) BabaAhmadi, R.; Ghanbari, P.; Rajabi, N. A.; Hashmi, A. S. K.; Yates, B. F.; Ariafard, A. *Organometallics* **2015**, *34*, 3186−3195.

(27) Ziegler, J. E.; Zdilla, M. J.; Evans, A. J.; Abu-Omar, M. M. *Inorg. Chem.* **2009**, *48*, 9998−10000.

DOI: 10.1021/acs.joc.6b02092
J. Org. Chem. 2016, 81, 9381−9388

(28) Bi, S.; Wang, J.; Liu, L.; Li, P.; Lin, Z. *Organometallics* **2012**, *31*, 6139−6147.
(29) Zeng, X.; Kinjo, R.; Donnadieu, B.; Bertrand, G. *Angew. Chem., Int. Ed.* **2010**, *49*, 942−945.
(30) Kozuch, S.; Shaik, S. *Acc. Chem. Res.* **2011**, *44*, 101.
(31) For examples of the application of an energetic span model, see: (a) Jiang, Y. − Y.; Yan, L.; Yu, H. − Z.; Zhang, Q.; Fu, Y. *ACS Catal.* **2016**, *6*, 4399−4410. (b) Dudnik, A. S.; Weidner, V. L.; Motta, A.; Delferro, M.; Marks, T. *Nat. Chem.* **2014**, *6*, 1100−1107. (c) Qiao, Y.; Wei, D.; Chang, J. *J. Org. Chem.* **2015**, *80*, 8619−8630.

DOI: 10.1021/acs.joc.6b02092
J. Org. Chem. 2016, 81, 9381−9388